Acta Cryst. (1999). B**55**, 507–516

A TEM study of long-period mica polytypes: determination of the stacking sequence of oxybiotite by means of atomic resolution images and Periodic Intensity Distribution (PID)

Toshihiro Kogure* and Massimo Nespolo†

Mineralogical Institute, Graduate School of Science, The University of Tokyo, 7-3-1 Hongo, Bunkyo-ku, Tokyo 113-0033, Japan. E-mail: kogure@min.s.u-tokyo.ac.jp

(*Received 17 June 1998; accepted 27 April 1999*)

Abstract

In this study it is shown that the stacking sequences in long-period mica polytypes (including a rare example of a mixed-rotation polytype, with a 36-layer long periodicity) can be unambiguously determined using atomic resolution images recorded down two zone axes separated by 30° (*e.g.* [100] and [3$\bar{1}$0]) at the same area. Uniformity of these stacking sequences in a large area is further confirmed by the correspondence between computed and observed Periodic Intensity Distributions (PIDs) in electron diffraction patterns. The appearance of long-period polytypes containing layers with different orientation parity may be explained by the coalescence of two small crystals during crystal growth.

1. Introduction

Polytypism of mica has been extensively investigated to reveal mica structure, stability fields and the formation mechanism. It is well known that polytypism of mica originates from the stacking of a 2:1 or *T–O–T* (Tetrahedra–Octahedral–Tetrahedral) unit layer, whose stacking vector can take six orientations (Smith & Yoder, 1956). To express these orientations, Zvyagin and coworkers (Zvyagin *et al.*, 1979; Zhukhlistov *et al.*, 1990) used six digits (1,2,...6; hereafter referred to as Z symbols) which correspond to the (001) projection, expressed in a space-fixed reference, of the intralayer displacement vectors connecting an interlayer site with the origin located in the octahedral site having (OH—F) groups in *trans*. The complete stacking vector is simply twice the intralayer displacement vector and is indicated by the same symbols (Zhukhlistov *et al.*, 1990).‡ Ross *et al.* (1966) used orientation-free, rotational symbols (RTW symbols), which represent the rotation between next layers as a multiple of 60° (0, ±1, ±2, 3); RTW symbols can be obtained as the difference between pairs of Z symbols. TS symbols (Takeda & Sadanaga, 1969) are used to compute the Periodic Intensity Distribution (PID) function (Takeda & Ross, 1995; Nespolo *et al.*, 1999).

Mica polytypes in which the position of any layer relative to the others and the transition from it to the adjacent ones are the same or equivalent for all layers are termed *homogenous polytypes* (Zvyagin, 1988) and were firstly derived by Smith & Yoder (1956), who termed them 'simple polytypes'. *Inhomogeneous polytypes* are those not obeying the above condition (Zvyagin, 1988): they appear almost exclusively in biotites and lithium micas (Nespolo, 1998*a*). Biotite is trioctahedral mica commonly occurring in igneous and metamorphic rocks. Ross *et al.* (1966) reported inhomogeneous polytypes with up to 23 layers in the repeat unit in an oxybiotite from Ruiz Peak, New Mexico. Bigi & Brigatti (1994) also described several long period polytypes in plutonic biotite from Valle del Cervo, Italy.

To identify the stacking sequence of mica polytypes, X-ray diffraction and oblique-texture electron diffraction (Zvyagin, 1967; Zvyagin *et al.*, 1979) were the main techniques used until recent times. Takeda (1967) and Takeda & Sadanaga (1969) derived the so-called Periodic Intensity Distribution (PID) function, which has been successfully applied to identify the stacking sequence of inhomogeneous polytypes in oxybiotite (Ross *et al.*, 1966) and taeniolite (Takeda, 1967). Nespolo *et al.* (1999) further refined this method and offered a new program to calculate PID from RTW symbols, in a uniquely defined axial setting (Nespolo *et al.*, 1998). This method determines the stacking sequences by comparing the observed and calculated intensity distribution, but the number of possible stacking sequences increases very quickly with the number of layers in a repeat unit (Mogami *et al.*, 1978; McLarnan, 1981). This approach thus requires a fairly long computation time when the number of layers is significantly large. Moreover, X-ray diffraction analysis is hindered by the presence of twins (Nespolo, Takeda & Ferraris, 1997; Nespolo, Takeda, Ferraris & Kogure, 1997; Nespolo, 1999) and by syntactic coalescence of different polytypes (Trigunayat, 1991).

† Present address: National Institute for Research in Inorganic Materials, 1-1 Namiki, Tsukuba-shi, Ibaraki 305-0044, Japan.

‡ This statement is not correct in the case of layers where the origin of the octahedral sheet is in one of the two sites having the (OH—F) groups in *cis*. Only a few examples of micas built by such a layer are known (*e.g.* Zhukhlistov *et al.*, 1996) and are not considered in this research.

On the other hand, Iijima & Buseck (1978) demonstrated that the stacking sequence of mica polytypes could be determined using high-resolution transmission electron microscopy (HRTEM). This technique has been successively applied by several research groups (*e.g.* Baronnet *et al.*, 1993). However, in these studies the specimens were observed down only one direction of [100], [110] or [1$\bar{1}$0], which are separated from each other by $n60^\circ$, and perfect three-dimensional stacking sequences could not be determined without applying restrictions about possible layer-stacking sequences (Iijima & Buseck, 1978). The results of those studies are still valid for subfamily A polytypes† (Backhaus & Ďurovič, 1984), which are polytypes consisting of layers described by Z symbols of the same parity, *i.e.* by layers related by 0 or $\pm120^\circ$ rotations only (0 or ±2 using RTW symbols). Actually, most of the mica polytypes found to date belong to subfamily A. Lithium micas are unusual in this respect, since they gave several examples of the $2M_2$ polytype, which belongs to subfamily B (Backhaus & Ďurovič, 1984). Subfamily B contains polytypes consisting of layers described by Z symbols of alternating parity, *i.e.* layers related by 180 or $\pm60^\circ$ rotations only (3 or ±1 using RTW symbols). Another example of subfamily B polytype (2*O* polytype) was discovered in anandite, a brittle mica with unusual chemical composition (Giuseppetti & Tadini, 1972; Filut *et al.* 1985). Besides, lithium micas also showed some examples of mixed-rotation polytypes, which are polytypes built by layers described by Z symbols of non-alternating different parity (Nespolo, 1999). If we determine the stacking sequences of mica polytypes which belong to subfamily B or mixed-rotation polytypes using HRTEM, the observation down another direction is necessary. Analyses of stacking sequences in layer silicates observed down [010], [310] or [3$\bar{1}$0], which are separated by $(2n-1)30^\circ$ from [100], [110] or [1$\bar{1}$0], have not been performed because they require higher resolution images to determine the stacking sequences. However, it has been recently demonstrated that determination of the stacking sequences in sheet silicates is successful by observing down these directions (Banfield & Murakami, 1998; Kogure & Banfield, 1998).

In this paper new very long-period polytypes are reported, including an ordered mixed-rotation polytype, discovered in an oxybiotite sample from the same Ruiz Peak rhyodacite in which Ross *et al.* (1966) identified several inhomogeneous polytypes by X-ray diffraction. The stacking sequence has been determined by HRTEM images recorded down two zone axes separated by 30° (*e.g.* [100] and [3$\bar{1}$0]) at the same area; this technique uniquely identifies the stacking sequence and the only ambiguity left is the possible presence of enantiomorphism. Although HRTEM images can directly determine the stacking sequence with ease, diffraction techniques are superior to confirm the uniformity of the stacking sequence in a large area (of the order of micrometers). PID analysis in electron diffraction patterns has thus also been performed to confirm that the stacking sequences determined by HRTEM are retained in large areas. Finally, a plausible formation mechanism of the long-period, mixed-rotation polytype is briefly discussed.

† Subfamily A polytypes have been termed ternary polytypes by Takeda & Ross (1995).

2. Materials and methods

Several oxybiotite crystals were gently crushed in an agate mortar and sandwiched together with epoxy resin by two glass slides. They were pressed by clips during the hardening of the epoxy resin to orient the oxybiotite platelets in parallel to the glass slides. Then they were cut into slices perpendicularly to the platelets. These slices were mechanically thinned and finished by ion-milling. Finally the specimens were carbon coated for TEM observation.

HRTEM observations were performed at 200 kV using a JEOL JEM-2010 electron microscope. The nominal C_s is 0.5 mm and the corresponding point resolution is ~2.0 Å, which is enough to resolve each silicon tetrahedra in a sheet, which are 2.6 Å apart if observed down [010], [310] or [3$\bar{1}$0]. Specimens can be tilted up to $\pm20^\circ$ about two axes in the microscope, which enables to observe some crystals down two types of zone axis separated by 30°. To record selected area diffraction (SAD) spots, which are very close to each other in the pattern of long-period polytypes, the size of the diffraction spots needs to be small and angular resolution should be increased. For these purposes, a Hitachi HF-2000 electron microscope with a cold field-emission (FE) gun was used operating at 100 kV. The cold FE gun is suitable to minimize the size of the diffraction spots owing to their small electron source size. Diffraction patterns were recorded to high-resolution imaging plates (IP, Fuji FDL-UR-V: 25 μm per pixel) to obtain digitized, quantitative intensity distributions in the patterns.

In order to determine the stacking sequences of polytypes directly from HRTEM images, the images on films were digitized using a CCD camera and processed using Gatan DigitalMicrograph 2.5 with the NCEM image processing package (Kilaas & Paciornik, 1995). To remove noisy contrast from amorphous materials the background subtraction filter (Kilaas, 1998) was applied to the images and, furthermore, residual noise was removed by masking the reciprocal spaces, except for reciprocal lattice rows along the c^* axis in the Fourier transform of the images. PID values from the stacking sequences obtained from HRTEM images were computed using the new program (*PTST*98) developed by Nespolo *et al.* (1999). This program starts from RTW symbols, computes Z and TS symbols and the space

group, checks the space disposition of symmetry elements and gives computed PID values in the most suitable axial setting.

3. Results and discussion

3.1. *HRTEM observations*

Selected area diffraction (SAD) revealed the existence of many kinds of polytypes, namely $1M$, $2M_1$, $3T$ (the latter being relatively rare) and several inhomogeneous polytypes, including long-period ones. The inhomogeneous polytypes can be easily identified using 'one-dimensional lattice fringe images' (Iijima & Buseck, 1978; Baronnet, 1992) with relatively lower magnification (×50 000–100 000) during observation. This method was first described by Iijima & Buseck (1978), forming the images with a crystal orientation tilted 'diagonally' by a few degrees from the principal zone axes, which are generally [100], [110] or [1$\bar{1}$0], and with a small objective aperture selecting the transmitted beam and several 00l reflections. Fig. 1(*a*) shows an example of such images, which indicates a long-period, inhomogeneous polytype. From these images it is easily recognized that the period of the polytype along c^* is ∼360 Å and the stacking sequence of each periodic unit is probably the same owing to their same contrast. The polytype in Fig. 1 has an unusual feature, as it also shows a periodic contrast in the image recorded down a direction close to [3$\bar{1}$0] (Fig. 1*c*). The reflections corresponding to $h \neq 0$(mod 3) and $k = 0$(mod 3) in the case of subfamily A and subfamily B polytypes are termed *family reflections* (or *family diffractions*; Ďurovič & Weiss, 1986). These recipocal lattice rows show one, two equally spaced and several reflections in the 0.1 Å^{-1} repeat of subfamily A, subfamily B and mixed-rotation polytypes, respectively (Nespolo, 1999). On the other hand, the remaining reflections are termed *non-family* reflections and are typical of each polytype (Ďurovič *et al.*, 1984). Fig. 1(*e*) shows the 13l reciprocal lattice row, on which several reflections are clearly seen. It is thus a non-family row and it identifies the polytype as a mixed-rotation one. Other inhomogeneous polytypes observed in this study all showed only one reflection in the 0.1 Å^{-1} repeat along these rows, and thus they belong to subfamily A: these polytypes show no distinct contrast when observed down the direction similar to that in Fig. 1(*c*).

Figs. 2(*b*) and 2(*c*) show atomic resolution images recorded down [100] and [3$\bar{1}$0], respectively, in the same area, with the corresponding one-dimensional lattice image (Fig. 2*a*) recorded down near [100], taken similarly to that in Fig. 1(*a*). The black arrow in Fig. 2(*b*) indicates the position of a cleaved surface, which is used as a marker to identify the same unit layer among these figures. The correspondence between the contrasts in Figs. 2(*b*) and 2(*c*) and atomic positions in the biotite structure were described in our previous papers (*e.g.* Kogure, 1997; Kogure & Banfield, 1998). The projection of the stacking vector of each layer can be traced as indicated with white arrows in Figs. 2(*b*) and 2(*c*), and the Z symbol of each layer can be determined by the two arrows of each layer. These analyses revealed that the inhomogeneous polytype under investigation has a 36-layer repeat unit; Z, RTW and TS symbols are given in Table 1. This polytype can be described as belonging to the $2M_1$ structural series, according to the definitions introduced by Takeda & Ross (1995). The same sample

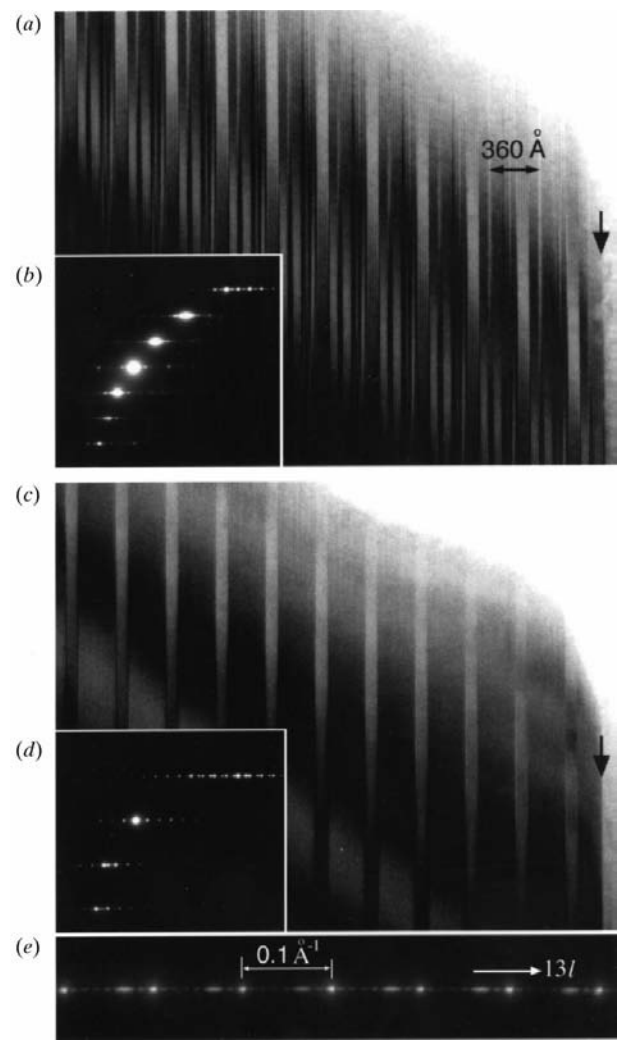

Fig. 1. (*a*) A one-dimensional lattice image of a 36-layer polytype observed down near [100]; (*b*) the corresponding SAD pattern. (*c*) A one-dimensional lattice image at the same area, but rotated about c^* by 30° from the crystal orientation in (*a*); (*d*) the corresponding SAD pattern. The arrows in (*a*) and (*c*) indicate a cleavage surface. (*e*) A magnified image of the 13l reciprocal lattice row in the SAD pattern recorded down [3$\bar{1}$0]. The appearance of several diffraction spots clearly proves the mixed-rotation nature of this 36-layer polytype.

Table 1. *Symbols describing the stacking sequence of the 36-layer mixed-rotation polytype*

n	Z	RTW	TS	*n*	Z	RTW	TS
1	2	2	*D**(10,−1)	19	6	−2	*D**(1,−1)
2	4	−2	*D**(−7,0)	20	4	−2	*D**(11,0)
3	2	2	*D**(3,−1)	21	2	2	*D**(−6,−1)
4	4	−2	*D**(13,0)	22	4	−2	*D**(4,0)
5	2	2	*D**(−4,−1)	23	2	0	*D**(−13,−1)
6	4	−2	*D**(6,0)	24	2	2	*D**(−3,1)
7	2	2	*D**(−11,−1)	25	4	−2	*D**(7,−1)
8	4	0	*D**(−1,0)	26	2	2	*D**(−10,1)
9	4	0	*D**(9,1)	27	4	−2	*D**(0,−1)
10	4	−2	*D**(−8,−1)	28	2	−1	*T**(10,1)
11	2	2	*D**(2,1)	29	1	2	*D*(2,0)
12	4	−2	*D**(12,−1)	30	3	−2	*D*(−6,0)
13	2	2	*D**(−5,1)	31	1	2	*D*(13,−1)
14	4	−2	*D**(5,−1)	32	3	−2	*D*(5,−1)
15	2	2	*D**(−12,1)	33	1	2	*D*(−3,1)
16	4	−2	*D**(−2,−1)	35	3	−2	*D*(−11,1)
17	2	2	*D**(8,1)	34	1	2	*D*(8,0)
18	4	2	*D**(−9,−1)	36	3	−1	*T*(0,0)

has revealed another long-period polytype: it is a 32-layer subfamily A polytype (Z symbols of the same parity), which can be described as belonging to the 3*T* structural series (Takeda & Ross, 1995; Fig. 3). The stacking sequence, identified in the same way as for the 36-layer unit, is given in Table 2. The space group of

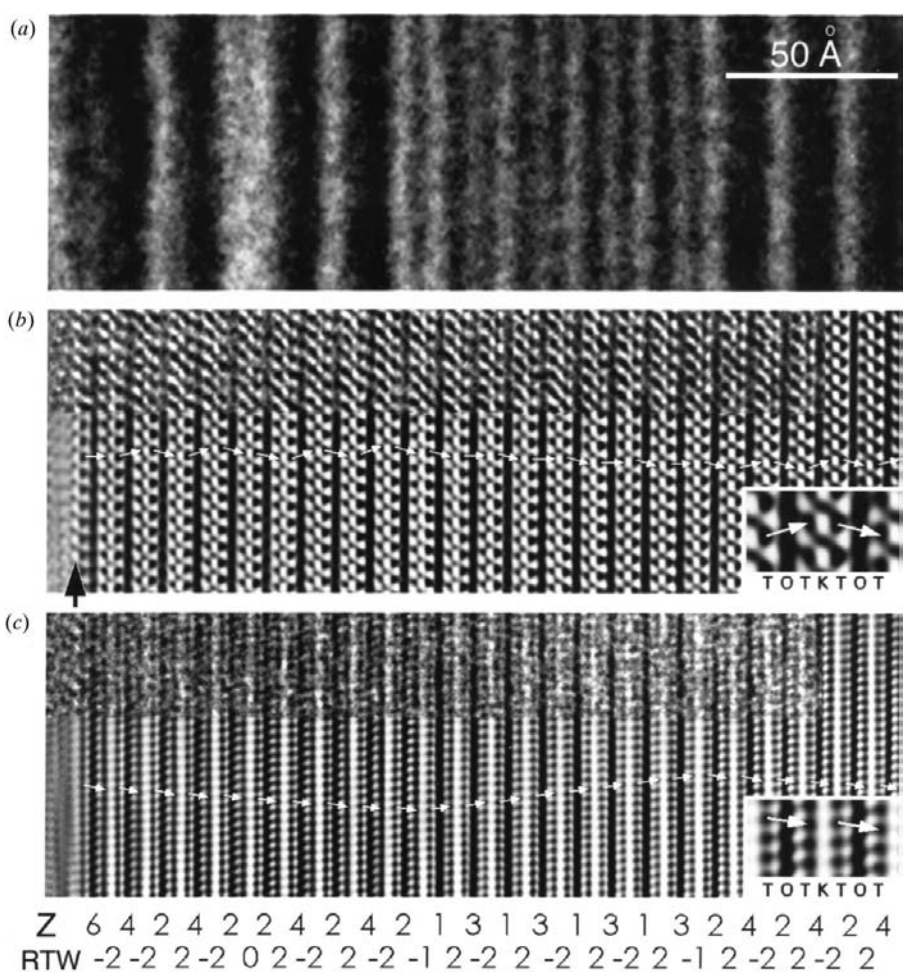

Fig. 2. (*a*) A magnified one-dimensional lattice image of the 36-layer polytype recorded down near [100], similar to Fig. 1(*a*). (*b*), (*c*) Unprocessed (top of the figure) and processed (bottom) atomic resolution images at the same area recorded down [100] (*b*) and [3$\bar{1}$0] (*c*). The determined Z and RTW symbols for each unit layer are also given at the bottom. The insets at the bottom-right in (*b*) and (*c*) are magnified images to show the correspondence between HRTEM contrast and atom positions, where T, O and K indicate tetrahedral sheet, octahedral sheet and potassium ions, respectively. The black arrow in (*b*) indicates a cleaved surface and white, fine arrows in (*b*) and (*c*) correspond to the projection of the stacking vector in each unit layer.

both polytypes is *C*1, derived on the basis of the symmetry rules for Z symbols developed by Zvyagin (1974, 1997). A *C* cell for triclinic polytypes is normally adopted for micas, since this cell is based on the two (pseudo)-orthohexagonal axes in the plane of the layer which is common to all polytypes.

These two polytypes have longer period and more complex stacking sequences than those reported by Ross *et al.* (1966) from the same sample. Several other polytypes with shorter periodicity have been found in this same sample, but all of them belong to subfamily A, as revealed by one-dimensional lattice images near [010], [310] or [3$\bar{1}$0] and SAD patterns of family reflections.

3.2. *Periodic Intensity Distribution*

The stacking sequence in a repeat unit of long-period inhomogeneous polytypes is unambiguously determined by HRTEM images, as shown in Fig. 2; besides, the one-dimensional lattice images such as those shown in Fig. 1 can reveal the uniformity of the determined sequence for a few tens of units. However, as thin crystals are easily bent and the diffraction contrast is very sensitive to the crystal orientation, it is not easy to discuss the uniformity of the stacking sequence of a polytype over a large area (order of micrometers). Diffraction techniques are more suitable to discuss such a problem.

Fig. 4(*a*) shows a SAD pattern of the 36-layer mixed-rotation polytype recorded down [100], using SA aperture selecting an area of ~2 μm in diameter, where only this polytype is expected (recording methods are described in the previous section). As shown in Fig. 4(*b*), the resolved diffraction spots corresponding to a period of 360 Å are identified and neither apparent streak nor extra spots are observed. Fig. 5 indicates line intensity profiles on 00*l* and 02*l* reciprocal lattice rows in the diffraction pattern in Fig. 4, obtained from an IP

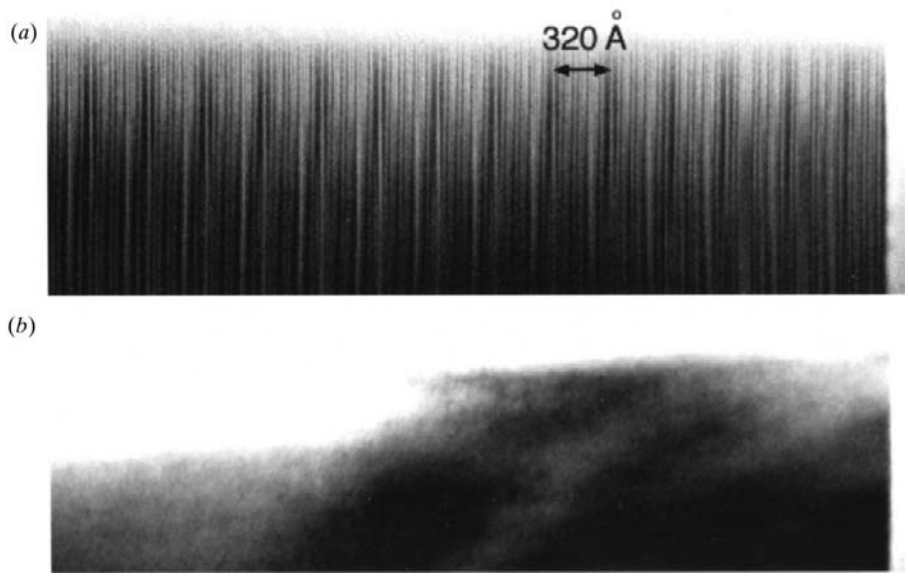

Fig. 3. A one-dimensional lattice image of a 32-layer, subfamily A polytype recorded down near [100] (*a*) and [3$\bar{1}$0] (*b*). Note that no distinct contrast is observed in (*b*), showing that this polytype belongs to subfamily A.

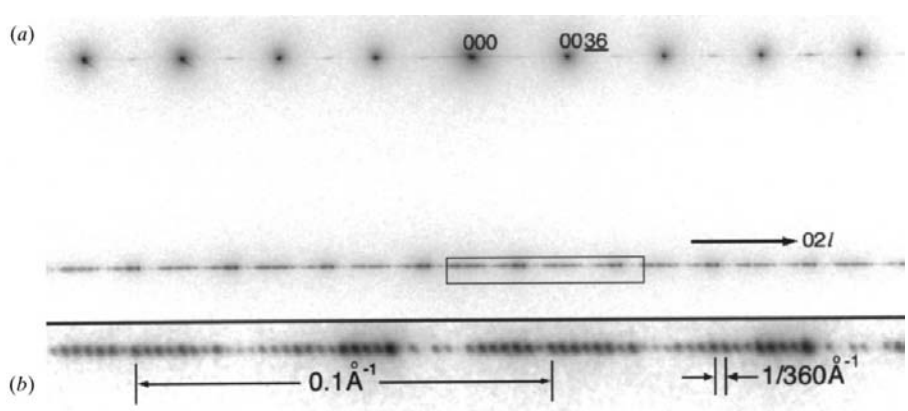

Fig. 4. (*a*) 0*kl* SAD pattern from the 36-layer polytype recorded on an imaging plate (IP). The diameter of the SA aperture corresponds to ~2 μm. The faint diffraction spots between 00*l* spots with 0.1 $Å^{-1}$ repeat are due to multiple diffraction. (*b*) Magnified image of the 02*l* reciprocal lattice row in the square box in (*a*). The separation of diffraction spots corresponds to 360 Å periodicity and no extra spots or apparent streak is observed.

Table 2. *Symbols describing the stacking sequence of the subfamily A 32-layer polytype*

n	Z	RTW	TS	*n*	Z	RTW	TS
1	6	2	*D*(0,0)	17	6	2	*D*(0,0)
2	2	−2	*D*(0,1)	18	2	2	*D*(0,1)
3	6	2	*D*(0,1)	19	4	2	*D*(0,0)
4	2	2	*D*(0,−1)	20	6	2	*D*(0,0)
5	4	−2	*D*(0,1)	21	2	2	*D*(0,1)
6	2	2	*D*(0,−1)	22	4	−2	*D*(0,0)
7	4	2	*D*(0,1)	23	2	2	*D*(0,1)
8	6	2	*D*(0,1)	24	4	2	*D*(0,0)
9	2	2	*D*(0,−)	25	6	2	*D*(0,0)
10	4	2	*D*(0,1)	26	2	2	*D*(0,1)
11	6	−2	*D*(0,1)	27	4	2	*D*(0,0)
12	4	2	*D*(0,0)	28	6	2	*D*(0,0)
13	6	2	*D*(0,0)	29	2	2	*D*(0,1)
14	2	−2	*D*(0,1)	30	4	−2	*D*(0,0)
15	6	−2	*D*(0,1)	31	2	2	*D*(0,1)
16	4	2	*D*(0,0)	32	4	2	*D*(0,0)

(imaging plate). Following Takeda & Ross (1995) the kinematical intensity ($|G^N|^2$) of non-family reciprocal rows for the *N*-layer mica can be expressed as

$$|G^N|^2 = |G_0|^2 \times |S^N|^2, \quad (1)$$

where $|G_0|$ is the Fourier transform of the unit layer. $|S^N|$ is the PID (Periodic Intensity Distribution) function, which is a type of fringe function (Lipson & Taylor, 1958) corresponding to the Fourier transform of the stacking sequence, obtained by removing the effect of intensity modulation of the layer transform from the structure factor. Equation (1) is valid on the whole subspace of the non-family reflections for polytypes belonging to both subfamilies, but it is restricted to the three planes 0*kl*, *hhl* and $hh\bar{l}$ for mixed-rotation polytypes (Nespolo *et al.*, 1999). Comparison of measured and calculated PID values on reciprocal lattice rows belonging to different planes is recommended to confirm the stacking sequence of subfamily B and mixed-rotation polytypes, and the adoption of a consistent axial setting significantly simplifies the comparison procedure (Nespolo *et al.*, 1999). In Fig. 6 the [110]* axes of the orthohexagonal C_1 setting and of the ^{9a}**F** settings (the setting in which PID is expressed; for details refer to Nespolo *et al.*, 1997, 1998) are shown in the SAD pattern recorded down [1$\bar{1}$0].

Generally, the wavelength of oscillation of $|G_0|^2$ is long enough compared with the period of the reciprocal

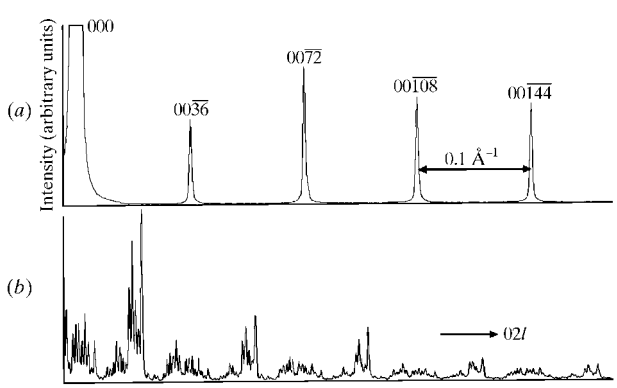

Fig. 5. The intensity distributions on 00*l* (*a*) and 02*l* (*b*) reciprocal lattice rows in Fig. 4.

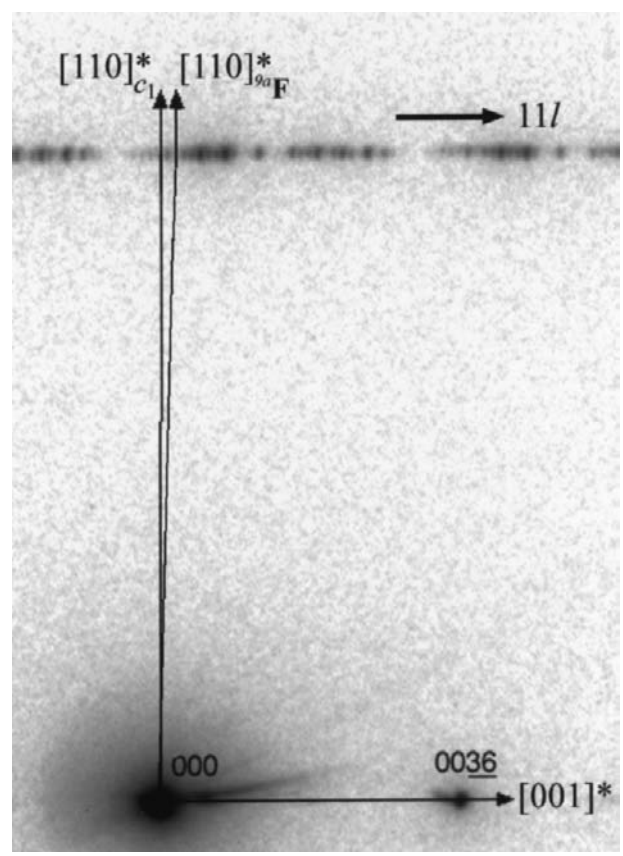

Fig. 6. [110]* axes of the C_1 and ^{9a}**F** axial setting, traced following the method described in Nespolo *et al.* (1998).

lattice nodes along c^* and is regarded as an envelope function modulating $|S^N|^2$. As is well known, the intensity distribution of electron diffraction is generally not kinematical. This fact clearly appears when comparing the calculated $|G_0|^2$ and the intensity profile on 00l reciprocal lattice row in Fig. 5(a). For instance, $I_{00\underline{72}}/I_{00\underline{36}}$ is ~0.08 by kinematical calculation and this value is close to unity in Fig. 5(a). However, the observed intensities of diffraction spots in a 0.1 Å^{-1} period show a good match with $|S^N|^2$ calculated by means of the stacking sequence determined by HRTEM analyses, indicating that *intensity ratios* between neighbouring diffraction spots are sufficiently preserved in the dynamical electron diffraction (Figs. 7a and 7b for the 02l reciprocal lattice row, and Figs. 7d and 7e for 11l). Although more theoretical study is needed to explain this phenomenon, it can be concluded that PID function is applicable to the electron diffraction of long-period mica polytypes. Fig. 7(c) also shows another example of calculated $|S^N|^2$ values for the 02l reciprocal lattice row, obtained by minimal modification of the determined stacking sequence (changing the TS symbol on one unit layer only). The experimental $|S^N|^2$ best matches that calculated from the HRTEM observation, showing that PID identifies the stacking sequence in a unique way.

3.3. *Origin of long-period, mixed-rotation polytypes*

Finally, the origin of the long-period, mixed-rotation polytype is considered. Fig. 8 shows the boundary where the 36-layer mixed-rotation polytype starts (or terminates) in the crystal. This is a one-dimensional lattice image similar to that in Fig. 1(c), where eight unit layers with odd-parity Z symbols (see Table 1) are identified as thin stripes. The right portion of the crystal from the boundary, which continues for several micrometers, wholly consists of the 36-layer polytype. The left side of the boundary, where no distinct contrast is observed, was revealed to be a subfamily A, 24-layer polytype which contains layers from nos 5 to 28 of the 36-layer polytype in Table 1. The 24-layer polytype can thus be regarded as a portion of the 36-layer one. At the boundary, there is a disorder with respect to the number of even-parity layers between the odd-parity eight layers (Fig. 8). From these observations it is inferred that the odd-parity eight layers were introduced from outside onto the mica surface where the 24-layer polytype was growing by spiral growth. The introduction of the odd-parity eight layers may have perturbed some portions of the spiral ledge and, after some transition period, a new 36-layer mixed-rotation polytype started to grow. In Fig. 9 a HRTEM image shows the region where the first odd-parity eight layers appear (the area indicated by the small box and by the white arrow in Fig. 8); Z symbols as determined from the image are indicated. The Z symbol of the unit layer just on the left of the odd-parity eight layers is identified to be 4, whereas it is expected to be 6

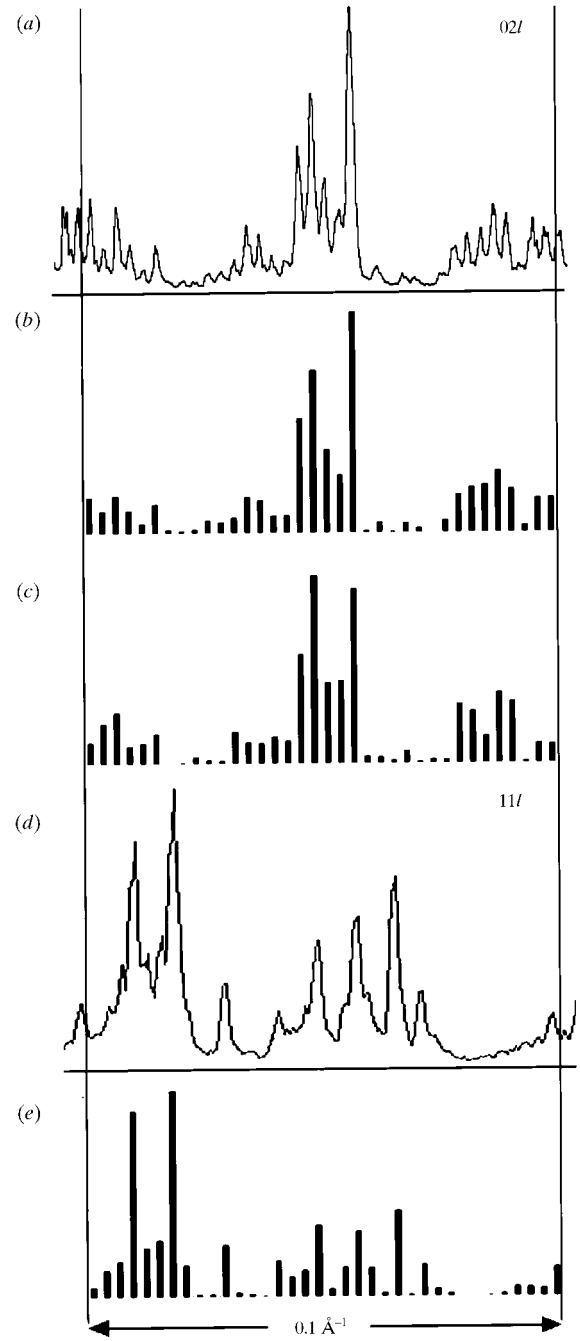

Fig. 7. (*a, d*) Observed intensity distribution on the diffraction patterns from the 36-layer polytype; (*b*), (*c*) and (*e*) calculated PID ($|S^N|^2$). (*a*) The intensity distribution in a 0.1 Å^{-1} period on the 02l row. (*b*) PID for the same row, computed from the stacking sequence determined by HRTEM, as shown in Table 1. (*c*) PID for the same row, computed from a stacking sequence with only a minimal modification with respect to the observed one [the TS symbol of layer no.7 has been altered from $D^*(-11, -1)$ to $D^*(-11, 1)$]. (*d*) The intensity distribution in a 0.1 Å^{-1} repeat on the 11l reciprocal lattice row. (*e*) PID for the same row, computed using the stacking sequences in Table 1.

in the 24-layer stacking sequence (layer no. 19 in Table 1). We presume that this unexpected stacking vector was generated by a lateral shift of the surface unit layer, to match the interlayer site of a foreign mica layer with the odd-parity Z symbol expanded on it. This lateral shift will probably have occurred through a growth defect (Nespolo, 1998) or a crystallographic slip in correspondence of the octahedral sheet (Takéuchi & Haga, 1971; Bell & Wilson, 1986; Takéuchi, 1997; Nespolo, 1998). According to Takeda & Ross (1995), this oxybiotite was formed by vapour growth in the cavities of lava at high temperature. Some biotite crystallites may nucleate on the same substrate of a different mineral. As they grow laterally they start to coalesce and begin to cooperatively grow (Sunagawa *et al.*, 1975). Two crystallites may happen to be rotated to each other by $n60^\circ$ and the interlayer site position may not coincide; if the mismatch is $b/3$ the necessity of compensating it arises (Bell & Wilson, 1977; Nespolo, 1998). If one crystallite is thicker than the other, when these two crystallites laterally attach a certain number of layers of the thicker crystallite protrude on the surface of the other one (Baronnet, 1973, 1978; Penn & Banfield, 1998). These layers can expand onto the second crystallite and modulate the spiral growth occurring there. Such coalescence may produce unusual polytypes, such as the long-period, mixed-rotation one discovered in this study. As discussed above, the long-period polytypes found in this sample, both mixed-rotation and subfamily A, have a longer period than those reported in previous works (Ross *et al.*, 1966; Takeda & Ross, 1995). The stacking sequences of these polytypes are hardly explained by the perfect or faulted matrix model (Baronnet, 1992). A new model for the genesis of such complex stacking sequences is now under study and will be presented elsewhere.

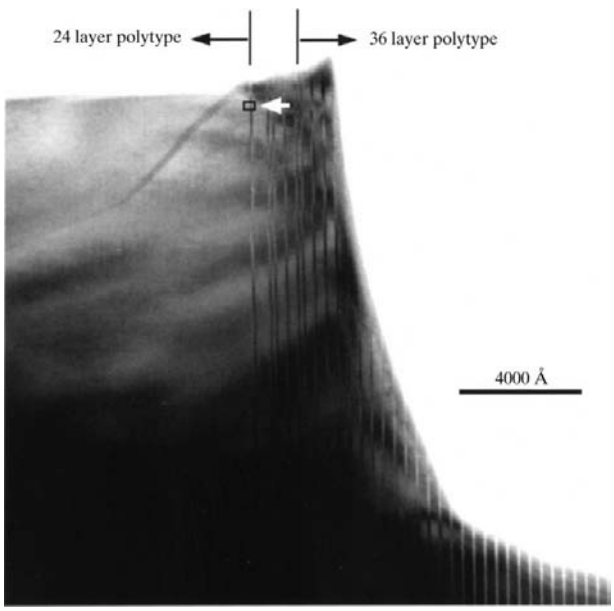

Fig. 8. A one-dimensional lattice image near the boundary between the 36-layer polytype and a 24-layer, subfamily A polytype. The beam direction is close to $[3\bar{1}0]$ (similar to that in Fig. 1*c*) and thin stripes on the right of the figure correspond to the eight unit layers with odd-parity Z symbols in Table 1. The small square box indicated by the white arrow corresponds to the area in Fig. 9.

4. Conclusions

This study has revealed the presence of several inhomogeneous polytypes in an oxybiotite sample from a locality where a wealth of polytypes was already found in previous studies. New polytypes and new results have been obtained, which can be summarized as follows.

HRTEM observing the same area down two zone axes has unambiguously revealed the existence and the stacking sequences of polytypes with a longer period

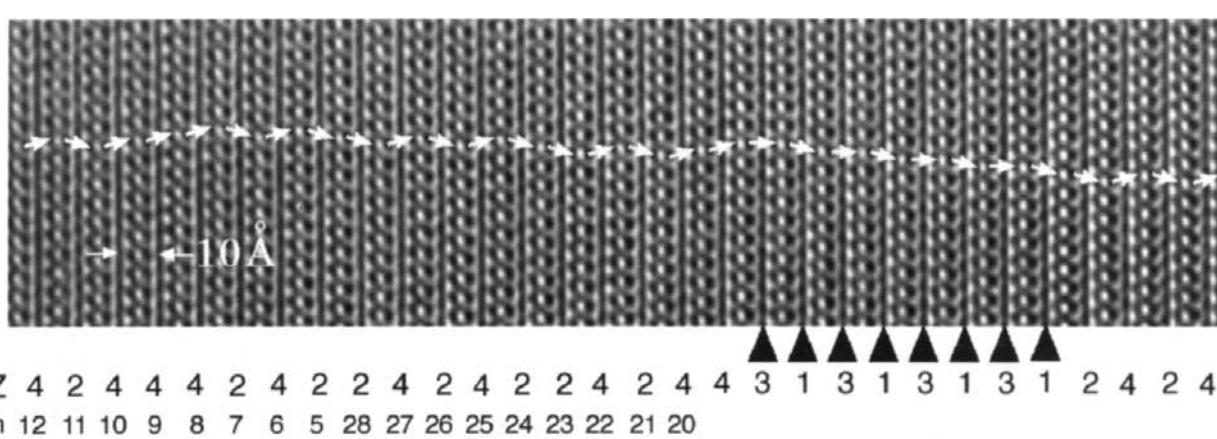

Fig. 9. The processed atomic resolution image at the small square box in Fig. 8 recorded down [100] and the Z symbol determined for each unit layer. The arrowheads indicate the eight unit layers with odd-parity Z symbols. The number below the Z symbols indicates the sequence layer numbers (n) in Table 1.

than those reported in previous studies. The 36-layer mixed-rotation polytype is of particular interest: it represents the mica polytype with the longest period found to date; it is one of the rare examples of mixed-rotation polytypes and the first found in a non-lithium mica. As is well known, TEM study also allows the recognition of the presence of small regions with a stacking sequence that differs from that of the matrix, and that do not appear on XRD patterns. These regions should not be termed *polytypes* unless their stacking sequence is regularly repeated a number of times, which is sufficient to support the existence of a growth memory. The 36-layer region found in this study is regularly repeated for more than 100 periods and thus it has the right of being defined a polytype.

This study has indicated that PID analysis of long-period mica polytypes is still valid in electron diffraction, although its intensity distributions are not kinematical. The intensity ratios between neighbouring spots in the observed diffraction patterns can be well reproduced by PID calculated using the stacking sequences determined by HRTEM.

The 36-layer mixed-rotation polytype was clearly formed through a polytypic transformation from a 24-layer subfamily A polytype. The unit layer situated between these two polytypes shows a stacking vector with a different orientation from those building each of the two polytypes. It may presumably be interpreted as a connecting layer originated from a lateral shift of the uppermost layer of the growing spiral, which occurred to match the interlayer site of foreign mica layers expanding on it. The mechanism generating these features seems to be a lateral coalescence of two crystallites rotated by $n60^\circ$ to each other, followed by expansion of some layers of one crystallite onto the surface of the other one.

We wish to thank Professor Hiroshi Takeda (Chiba Institute of Technology) and Professor Jillian F. Banfield (University of Wisconsin–Madison) for many important discussions. We are also grateful to Professor Yoshio Takéuchi (Nihon University), Professor Boris B. Zvyagin (IGEM, RAS, Moscow), Professor Giovanni Ferraris (University of Torino), Professor Slavomil Ďuroviè (Slovak Academy of Sciences, Bratislava) and Professor Stefano Merlino (University of Pisa) for their suggestions. One of us (MN) is deeply indebted to Professor Masamichi Miyamoto (University of Tokyo) and Professor Yasunari Watanabe (Teikyo Heisei University) for their constant encouragement. The sample was kindly provided by Dr Malcom Ross (US Geological Survey), to whom we express our gratitude. The electron microscopy was performed in the Electron Microbeam Analysis Facility of the Mineralogical Institute, the University of Tokyo. This research has been partly developed during a Doctoral Program (MN) supported by the Japanese Ministry of Education, Science and Culture.

References

Backhaus, K.-O. & Ďurovič, S. (1984). *Clays Clay Miner.* **32**, 453–463.

Banfield, J. F. & Murakami, T. (1998). *Am. Mineral.* **83**, 348–357.

Baronnet, A. (1973). *J. Cryst. Growth*, **19,** 193–198.

Baronnet, A. (1978). *Prog. Cryst. Growth Charact.* **1**, 151–211.

Baronnet, A. (1992). *Minerals and Reactions at the Atomic Scale: Transmission Electron Microscopy/MSA Rev. Mineral.*, edited by P. R. Buseck, Vol. 27, pp. 231–288. Washington, DC: Mineralogical Society of America.

Baronnet, A., Nitsche, S. & Kang, Z. C. (1993). *Phase Transit.* **43**, 107–128.

Bell, I. A. & Wilson, C. J. L (1977). *Phys. Chem. Miner.* **2**, 153–169.

Bell, I. A. & Wilson, C. J. L. (1986). *Bull. Mineral.* **109**, 163–170.

Bigi, S. & Brigatti, M. F. (1994). *Am. Mineral.* **79**, 63–72.

Ďurovič, S. & Weiss, Z. (1986). *Bull. Mineral.* **109**, 15–29.

Ďurovič, S., Weiss, Z. & Backhaus, K.-O. (1984). *Clays Clay Miner.* **32**, 454–474.

Filut, M. A., Rule, A. C. & Bailey, S. W. (1985). *Am. Mineral.* **70**, 1298–1308.

Giuseppetti, G. & Tadini, C. (1972). *Tschermaks Mineral. Petrogr. Mitt.* **18**, 169–184.

Iijima, S. & Buseck, P. R. (1978). *Acta Cryst.* A**34**, 709–719.

Kilaas, R. (1998). *J. Microscopy*, **190**, 45–51.

Kilaas, R. & Paciornik, S. (1995). *Proc. MSA*, **46**, 628–629.

Kogure, T. (1997). *Mineral. J.* **19**, 155–164.

Kogure, T. & Banfield, J. F. (1998). *Am. Mineral.* **83**, 925–930.

Lipson, H. & Taylor, C. A. (1958). *Fourier Transforms and X-ray Diffraction*, 76p. London: Bell.

McLarnan, T. J. (1981). *Z. Kristallogr.* **155**, 247–268.

Mogami, K., Nomura, K., Miyamoto, M., Takeda, H. & Sadanaga, R. (1978). *Can. Mineral.* **16**, 427–435.

Nespolo, M. (1998). Doctoral dissertation, 257 pp. University of Tokyo.

Nespolo, M. (1999). *Mineral. J.* **21**, 53–85.

Nespolo, M., Takeda, H. & Ferraris, G. (1997). *Modular Aspects of Minerals/EMU Notes in Mineralogy*, edited by S. Merlino, Vol. 1, pp. 81–118. Budapest: Eötvös University Press.

Nespolo, M., Takeda, H. & Ferraris, G. (1998). *Acta Cryst.* A**54**, 348–356.

Nespolo, M., Takeda, H., Ferraris, G. & Kogure, T. (1997). *Mineral. J.* **19**, 173–186.

Nespolo, M., Takeda, H., Kogure, T. & Ferraris, G. (1999). *Acta Cryst.* A**55**, 659–676.

Penn, R. L. & Banfield, J. F. (1998). *Science*, **281**, 969–971.

Ross, M., Takeda, H. & Wones, D. R. (1966). *Science*, **151**, 191–193.

Smith, J. V. & Yoder, H. S. (1956). *Mineral. Mag.* **31**, 209–235.

Sunagawa, I., Koshino, Y., Asakura, M. & Yamamoto, T. (1975). *Fortschr. Miner.* **52**, 217–224.

Takeda, H. (1967). *Acta Cryst.* **22**, 845–853.

Takeda, H. & Ross, M. (1995). *Am. Mineral.* **80**, 715–724.

Takeda, H. & Sadanaga, R. (1969). *Mineral. J.* **5**, 434–449.

Takéuchi, Y. (1997). *Topochemical Cell-Twinning. A Structure-Building Mechanism in Crystalline Solids*, 319 pp. Tokyo: Terra Publishing Co.

Takéuchi, Y. & Haga, N. (1971). *Mineral. Soc. Jpn Spec. Pap.* **1**, 74–87 (Proc. IMA-IAGOD Meetings '70, IMA Vol.).

Trigunayat, G. C. (1991). *Solid State Ion.* **48**, 3–70.

Zhukhlistov, A. P., Dragulescu, E. M., Rusinov, V. L., Kovalenker, V. A., Zvyagin, B. B. & Kuz'mina, O. V. (1996). *Zap. Vseross. Min. Obshch. (Proc. Russian Mineral. Soc.)*, **125**, 47–54 (in Russian, with English Abstract).

Zhukhlistov, A. P., Zvyagin, B. B. & Pavlishin, V. I. (1990). *Sov. Phys. Crystallogr.* **35**, 232–236.

Zvyagin, B. B. (1967). *Electron Diffraction Analysis of Clay Mineral Structures*, XVI + 364 pp. New York: Plenum Press.

Zvyagin, B. B. (1974). *2nd Eur. Cryst. Meet. Collect.* Abstracts, Keszthely, pp. 162–164.

Zvyagin, B. B. (1988). *Comput. Math. Appl.* **16**, 569–591.

Zvyagin, B. B. (1997). *Modular Aspects of Minerals/EMU Notes in Mineralogy*, edited by S. Merlino, Vol. 1, pp. 345–372. Budapest: Eötvös University press.

Zvyagin, B. B., Vrublevskaya, Z. V., Zhukhlistov, A. P., Sidorenko, O. V., Soboleva, S. V. & Fedotov, A. F. (1979). *High-Voltage Electron Diffraction in the Study of Layered Minerals*, 223 pp. Moscow: Nauka Press (in Russian).